ISSN 0021-3640, JETP Letters, 2025, Vol. 121, No. 4, pp. 306–314. © The Author(s), 2025. This article is an open access publication.
Russian Text © The Author(s), 2025, published in Pis'ma v Zhurnal Eksperimental'noi i Teoreticheskoi Fiziki, 2025, Vol. 121, No. 4, pp. 321–329.

BIOPHYSICS

Effect of Selenium, Copper and Silver Microparticles Obtained in Viscous Media on the Gram-Positive and Gram-Negative Bacteria Survival

I. N. Saraeva[a,*] (ORCID: 0000-0003-2362-023X), E. R. Tolordava[a] (ORCID: 0000-0002-9920-2432), R. A. Khmelnitsky[a], S. N. Shelygina[a], D. S. Pozdnyakova[b], A. A. Nastulyavichus[a], E. N. Rimskaya[a] (ORCID: 0000-0001-7802-0720), and A. E. Rupasov[a] (ORCID: 0000-0002-4443-5765)

[a] *Lebedev Physics Institute, Russian Academy of Sciences, Moscow, 119991 Russia*

[b] *National Research Nuclear University MEPhI (Moscow Engineering Physics Institute), Moscow, 115409 Russia*

*****e-mail: saraevain@lebedev.ru*

Received December 10, 2024; revised December 13, 2024; accepted December 13, 2024

The work presents a multiparametric analysis of the effect of antibacterial nanogels based on nano- and (sub)microparticles of silver, copper and selenium on single- and multicomponent biofilms of gram-positive bacteria *Staphylococcus aureus*, *Staphylococcus epidermidis*, as well as gram-negative bacteria *Escherichia coli*, *Klebsiella pneumoniae*, and *Pseudomonas aeruginosa*. Nanogels are based on glycerol, silicone oil and Vaseline, which are low-costing biocompatible materials, suitable for use in wound dressings. The active components are bactericidal Ag, Cu, and Se nanoparticles. Nanogels and their effect on the bacterial biofilms were studied by standard microbiological inoculations, as well as Fourier transform infrared spectroscopy methods, followed by principal component analysis. After the treatment of biofilms with nanogels, a decrease in the bacterial population up to 99% was observed. Principal component analysis demonstrated the ability to differentiate viable from nonviable bacteria.

DOI: 10.1134/S0021364024605190

1. INTRODUCTION

After the formation of wound, its almost immediate contamination with pathogenic microorganisms begins, which is why infections and inflammatory process are a serious problem in medicine. The complications that arise slow down wound healing and can also lead to the need for intensive antibiotic therapy, which worsens the general condition of the patient and poses a risk of strain mutation with the acquisition of resistance to the certain type of antibiotic. With long-term complications, the formation of biofilms may start in wounds. Biofilms are bacterial communities located in an exopolymer matrix [1, 2], which provides optimal conditions for their existence and additional protection from the antibiotics used: even if a certain drug is highly effective against a planktonic culture of a particular type, it may not affect the same type of bacteria in the form of a biofilm. Thus, the formation of biofilms can lead to a decrease in the effectiveness or complete leveling of treatment, as well as to the appearance of non-healing chronic wounds.

Currently, bacteria are becoming resistant to a number of antibiotics, which is why the search for bactericidal agents that eliminate such mutations is becoming relevant. Nanoparticles (NPs) are a good alternative to modern antibiotics and have proven effectiveness in combating both planktonic forms of bacteria and single- and multi-component biofilms [3, 4]. Modern research is carried out using the following main methods for NPs manufacturing: chemical synthesis, the use of plant extracts, and laser ablation (LA) in liquid [5–8]. The popularity of these methods is justified by their simplicity, good stability of the obtained NPs and low environmental impact. Thus, more and more works appear on the topic of NP generation by using plant extracts and even bacterial strains. The disadvantages of these methods include the complexity of extract preparation (collection of plants, grinding, extraction), as well as the separation of bacterial cultures from the obtained NPs. The disadvantages of chemical synthesis include the toxicity of some reagents and the complexity of the resulting colloidal solution purification. Unlike these methods, LA in liquid is a universal way for one-step NPs production in various solvents. The mechanisms of NPs formation in the LA process have been studied for several decades [9, 10]. NPs of a wide range of materials have been obtained in various environments using laser systems with femto-, pico-, and nanosecond pulse widths [11, 12]. However, femto- and picosecond lasers are characterized by high cost and often

induce difficulties in setup and maintenance, and therefore the use of industrial nanosecond markers, which do not require lengthy training of specialized personnel to work with them, is a more profitable and simple solution.

The mechanism of NPs formation during LA with nanosecond pulses has been studied in detail. The main stages include the formation of plasma and vapor bubble above the surface of the ablated target, the nucleation of NPs during the expansion and collapse of the bubble, the formation of a colloidal solution and the interaction of NPs with subsequent laser pulses (fragmentation), and the dynamics of the expansion and collapse of the bubble is largely affected by the viscosity of the surrounding medium.

There are many works that describe the formation of NPs in deionized water and alcohols [13, 14], but the production of NPs in viscous liquids is less covered in the literature [15]. Nevertheless, single-step preparation of NPs with a strong bactericidal effect (silver, copper, selenium) in viscous media is a promising method for the rapid and efficient production of nanogels that are potentially applicable for chronic wound infections' treatment.

This paper presents a multiparametric analysis of the effect of antibacterial nanogels based on silver, copper and selenium nano- and (sub)microparticles on the cell membrane and secondary structure of proteins in single- and multi-component biofilms of gram-positive bacteria Staphylococcus aureus (SA), Staphylococcus epidermidis (SE), and gram-negative bacteria Escherichia coli (EC), Klebsiella pneumoniae (KP) and Pseudomonas aeruginosa (PA). The nanogels are based on glycerol, silicone oil and Vaseline, which are widespread, biocompatible and inexpensive materials, also suitable for use in wound dressings. The active components are toxic Ag, Cu and Se NPs. Nanogels and their effect on the biofilms were studied using standard microbiological cultures, as well as infrared (IR) Fourier spectroscopy and principal component analysis (PCA).

2. EXPERIMENTAL DETAILS

The selected nanogel bases included glycerol (distilled, food additive E442, "Glycerine Solutions"), Vaseline (Megacos Co., Ltd, Gyeonggi-do), silicone oil (technical silicone grease PMS-100, "Komrek"). Deionized water and isopropyl alcohol (IPA) were used for comparison of antibacterial effect.

One-step preparation of nanogels was possible in glycerol, silicone oil, water and IPA. Vaseline was melted before ablation using a blow dryer at a temperature of 226°C. Bulk targets Ag (purity 99.999%), Cu (purity 99.99%) or Se (purity 99.999%) were placed in a glass beaker under the 2-mm layer of deionized water, IPA, glycerol, silicone oil or melted Vaseline, and laser system HTF MARK with wavelength 1064 nm and pulse width 120 ns was used for NPs fabrication. Laser radiation was focused on the target surface with F-theta objective lens (focusing length $F = 70$ mm) in a spot with diameter ≈ 50 μm, and raster-scanning with laser beam was implemented with constant speed 500 mm/s, repetition rate 20 kHz and laser energy 0.9 mJ across the 15×10-mm region with filling 10 lines/mm for 600 times. In the case of NPs' fabrication in Vaseline, the temperature increase caused by the absorption of laser radiation was sufficient to maintain its transparency and liquid state.

The obtained colloidal solutions of NPs in water, isopropyl alcohol, glycerol and silicone oil were characterized by UV-vis spectroscopy. The characterization of solutions obtained in Vaseline was carried out visually. The analysis of NPs by scanning electron microscopy (SEM) (Tescan) and energy-dispersive X-ray spectroscopy (EDS) was carried out after drying the NPs colloids on polished silicon plates.

Biofilms of SA, SE, EC, KP, PA bacteria were grown using the overnight broth cultures, diluted by 1 : 100 in LB medium (Miller, AppliChem). 2 mL was taken from each diluted culture and placed in the 24-well plates and filled with round plates of CaF_2 ($d = 1$ cm) or Au films, magnetron-sputtered on silicon substrates in argon medium (0.8×0.8 cm). For the growth of multi-component biofilms additional aliquots of several strains were placed in each well. Biofilms' growth was implemented by putting the plate in a thermostat with temperature 37°C for 48 h. For the further spectroscopic analysis, the nutrient broth was removed from the substrates with grown biofilms by rinsing it three times with saline.

Fourier-IR spectra were acquired with the use of IR spectrophotometer V-70 (Brucker) in the range 800–3500 cm^{-1} with 4 cm^{-1} resolution in vacuum camera using 2-mm diaphragm. CaF_2 substrates were used for the IR transmittance measurement, whereas IR reflectance was measured on Au films, sputtered on Si substrates. Up to 5 spectra were registered for the 5 samples of each type, with the resulting spectra number for each sample equaling 25. After the measurement, transmittance spectra were recalculated to optical density, whereas reflectance spectra were recalculated to absorbance spectra, and all spectra were normalized on the IR line of α-helices in amide I 1654 cm^{-1} [16].

Averaged IR spectra of each sample were approximated using the Lorentz function in the OriginPro software:

$$y = y_0 + \frac{2A}{\pi}\frac{w}{4(x - x_c)^2 + w^2}, \quad (1)$$

where y_0 is the baseline, A is the area under the curve, w is the FWHM of the band, and x_c is the position of the peak maximum (central frequency in inverse centimeters).

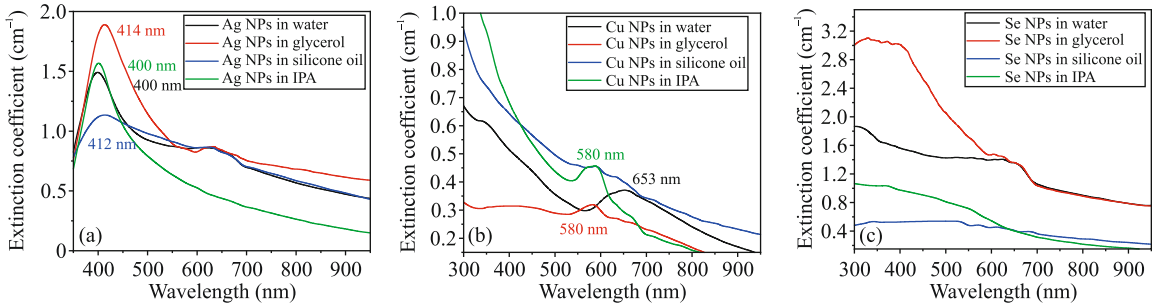

Fig. 1. (Color online) UV-vis extinction coefficient spectra of (a) Ag, (b) Cu, and (c) Se NP colloids in (black lines) deionized water, (red lines) glycerol, (blue lines) silicone oil, and (green lines) IPA.

Detection of the bands (hidden peaks) was implemented by finding the local maxima of the second derivative with Savitzky–Golay smoothing. The resulting values (central frequencies of the second derivative maxima x_c) were fixed, after which all peaks were approximated by the Lorentz approximation (1), and the values of the bandwidth w and the area under the curve A were obtained. The standard deviation was estimated by the program in accordance with the noise level estimate and the residual error value. Analysis of the amide I line, to the intensity of which the spectra were normalized, remained possible due to the influence of the line width on the total area under the curve.

Principal component analysis (PCA) was performed using OriginPro software. Smoothed and normalized IR optical density spectra were divided into two ranges: 1150–1800 cm^{-1} (spectral fingerprint region) and 2750–3250 cm^{-1} (region of membrane proteins and lipids molecular vibrations). For each spectral data range, PCA analysis was performed with the selection of 4 components, after which the dependences of the component loadings PC1 (Principal component 1) versus PC2 (Principal component 2) were plotted. The loadings describe the relationship of the variables with the components, and the contribution of the variables to the variability along the component is stronger, the greater the modulus of their loading is. The sign of the loading means the direction of change of the original variable along the principal component, therefore, the PC1 coefficients were further plotted as a graph with an abscissa corresponding to the wave numbers, and positive and negative PC1 loadings were identified, correlating with the spectra of the second derivatives and responsible for the classification of viable and nonviable bacteria.

3. RESULTS AND DISCUSSION

3.1. Characterization of Nanoparticles

The UV-visible optical density spectra of pure glycerol and silicone oil had no prominent features. The spectra of Ag, Cu, and Se NPs in water, IPA, glycerol, and silicone oil are shown in Fig. 1. Silver NPs demonstrate a peak corresponding to the plasmon resonance in the 400 nm region. This peak in glycerol, silicone oil, and IPA is located at wavelengths of 414, 412, and 400 nm, respectively. Usually, a shift of the resonance peak in the region of longer wavelengths indicates an increase in the average diameter of NPs. Copper NPs in water, glycerol, IPA, and silicone oil demonstrate a peak at 653, 580, 580 nm, and a broad wing in the region of 550–650 nm, respectively. The optical density spectra of selenium NPs in all the used media demonstrate broad absorption bands in the 300–400 nm region. The presence of plasmon resonance peaks in all obtained colloids proves the formation of NPs in solvents. The UV-visible optical density spectrum of pure glycerol and silicone oil had no visible features.

According to SEM characterization, all the obtained particles have a spherical shape (Supplementary Materials, Figs. S1–S6), except for selenium NPs prepared in silicone oil (see Fig. 2), which had a form of nanoneedles' conglomerates. In most cases, NPs obtained in organic media exhibit high carbon content (Supplementary Materials, Tables S1–S6).

The particle sizes varied from nano- to (sub)microscale fractions (Table 1).

According to the obtained data, laser ablation of NPs in silicone oil leads to the formation of (sub)microparticles. Micro-sized fractions are also observed after ablation in isopropyl alcohol, which is associated with the instability of the obtained solutions and rapid aggregation of NPs.

The colloids of gold, silver, copper, and selenium NPs obtained in the Vaseline medium are shown in Fig. S7 in the Supplementary Materials. Evidently, the color of the colloids corresponds to the plasmon resonances in silver, gold, and copper, as well as to the color of selenium NPs obtained in other solvents (see Fig. S7a). Visualization of the NPs using an optical microscope confirms the formation of selenium submicroparticles in the Vaseline medium (see Fig. S7b).

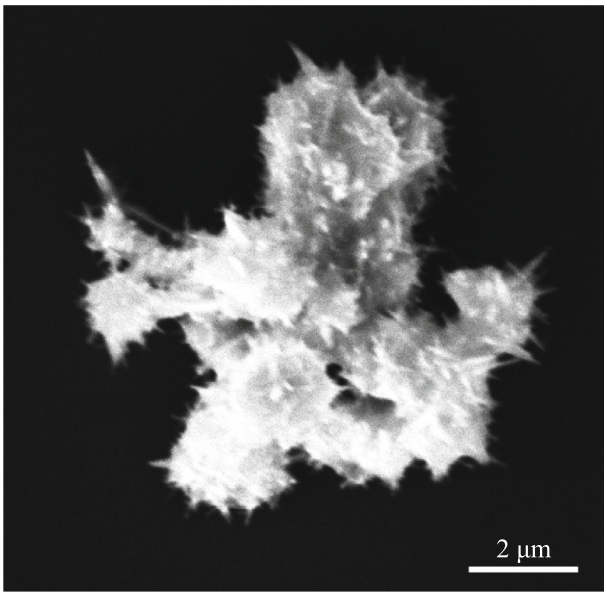

Fig. 2. SEM image of selenium NPs obtained by LA of a bulk target in silicone oil.

3.2. Microbiological Analysis of the Antibacterial Effect of Nanoparticles

The antimicrobial efficiency analysis of nanogels on biofilms was carried out using the strains SA, PA, EC, SE, KP and their combinations SA + SE + PA, SE + EC and EC + KP. The first stage involved growing biofilms on CaF_2 substrates and Au films deposited on silicon plates (Section 2). The substrates were then placed in sterile 24-well plates filled with nanogels and kept for 1 hour, after which the bacteria were washed off and inoculated to determine the number of CFU/mL (colony forming units per milliliter). Gels without NPs did not exhibit a bactericidal effect, whereas the reduction in the bacterial population after treatment with gels containing silver, copper and selenium NPs reached 99% (see Fig. 3).

The efficiency of silver, copper and selenium NPs in water has been demonstrated previously and confirmed in our experiments. Ag NPs obtained in glycerol also showed a prominent antibacterial effect: the bacterial population decreased by four orders of magnitude in SE, by two orders of magnitude in PA and KP. In combined biofilms, the effect reached three orders of magnitude. The decrease in CFU/ml after treatment with Ag NPs obtained in silicone oil was one order of magnitude on average. Cu NPs in glycerol suppressed bacterial growth by one (EC, SE + EC) to two orders of magnitude (SE, PA, EC + KP). Treatment of biofilms with copper nanoparticles in silicone oil was less effective and led to a decrease in CFU/mL values by one order of magnitude in SE, PA, SE + EC, EC + KP. Selenium NPs in glycerol reduced the population by one order of magnitude in SA, PA, EC, SA + SE + PA, EC + KP. The greatest effect by three and four orders of magnitude was observed in SE and KP, respectively. Treatment of biofilms with selenium NPs in silicone oil led to a decrease in CFU/mL by three orders of magnitude in SA and SA + SE + PA, and by two orders of magnitude in SE, EC, KP, and EC + KP. Thus, the efficiency of NPs during their generation in viscous media was maintained and even increased in the case of selenium ablation.

3.3. Infrared Spectroscopy Analysis of the Antibacterial Effect of Nanoparticles

The data from the bacteriological inoculation were illustrated by IR transmittance and reflectance spectroscopy (Supplementary Materials, Table S7). After processing the optical density and absorbance IR spectra, the central peak positions x_c, their FWHM, and the area under the curve A were obtained. The FWHM and area values were plotted as a 2D contour

Table 1. Particle sizes determined by dynamic light scattering

Type of colloid	Size fraction 1, nm	Size fraction 2, nm	Size fraction 3, nm
Ag NPs in water	7.2	96	
Ag NPs in isopropanol	6.1	129	1853.5
Ag NPs in glycerol	35		
Ag NPs in silicon oil			1394.9
Cu NPs in water	18.5	469	
Cu NPs in isopropanol	2.97		
Cu NPs in glycerol	2.39	84.7	
Cu NPs in silicon oil		542.3	
Se NPs in water	38.2	315.3	
Se NPs in isopropanol	2.81		7579.1
Se NPs in glycerol		62.7	
Se NPs in silicon oil			3065.4

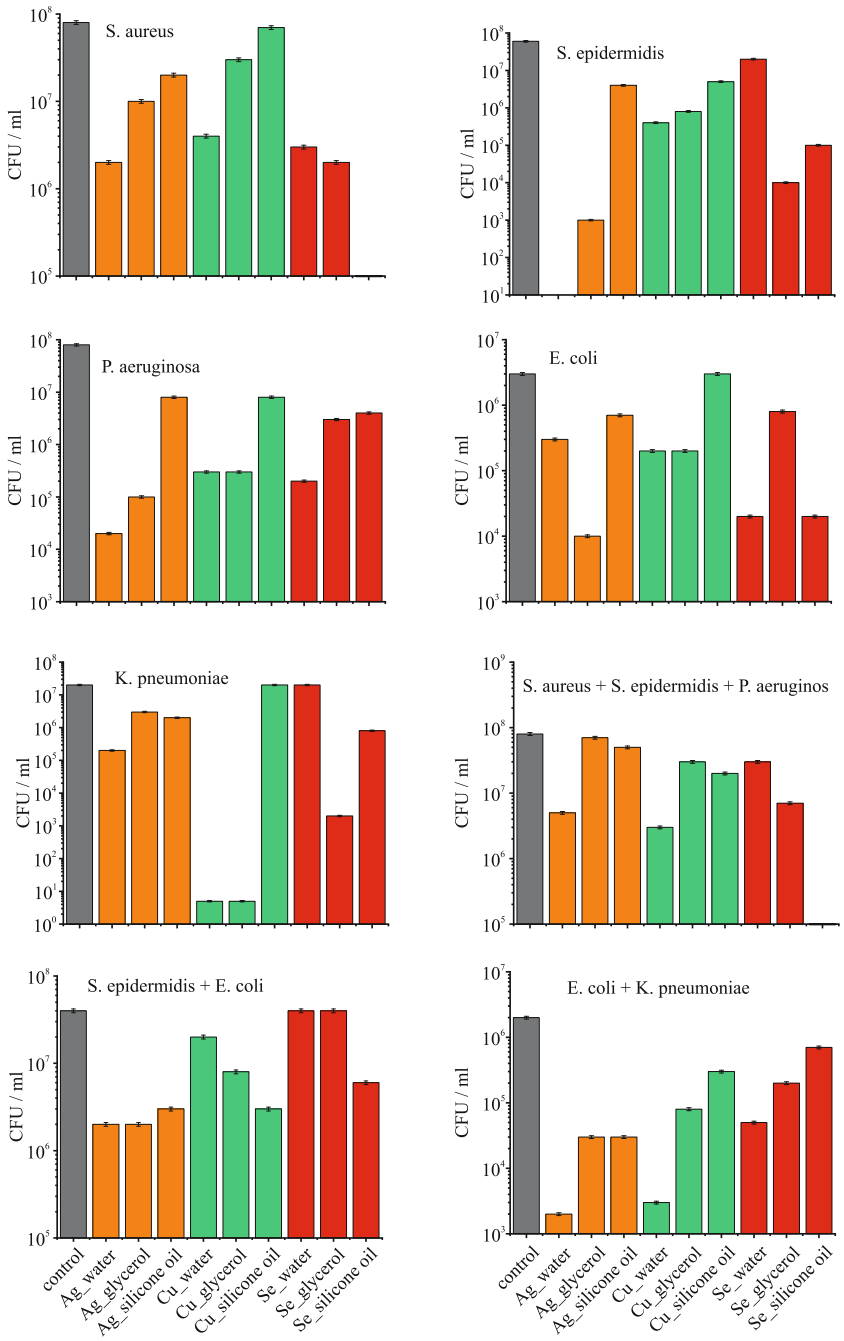

Fig. 3. (Color online) Viability of bacterial single- and multi-component biofilms in CFU/ml values: (gray bars "control") without NP treatment and after application of (orange bars) silver NPs, (green bars) copper NPs, and (red bars) selenium NPs in water, glycerol and silicone oil.

graph (see Fig. 4), on the abscissa of which the control (untreated) biofilms are designated by the abbreviations of the corresponding bacteria: *S. aureus*, *S. epidermidis*, *P. aeruginosa*, *E. coli*, *K. pneumoniae*, *S. epidermidis* + *E. coli*, *S. aureus* + *S. epidermidis* + *P. aeruginosa*, *E. coli* + *K. pneumoniae*. Biofilms treated with silver NPs are designated by the abbreviations of the names of the corresponding bacteria with the addition of the NP types: Ag, Cu, and Se. The ordinate axis represents the designations of molecular vibrations, which correspond to the IR bands. Thus, the change in the areas (see Figs. 4a, 4c) and peak widths (see Figs. 4b, 4d) of bacteria is monitored before treatment (SA, SE, PA, EC, KP, SE + EC, SA + SE + PA, EC + KP), after treatment with silver NPs (SA Ag, SE Ag, PA Ag, EC Ag, KP Ag, SE + EC

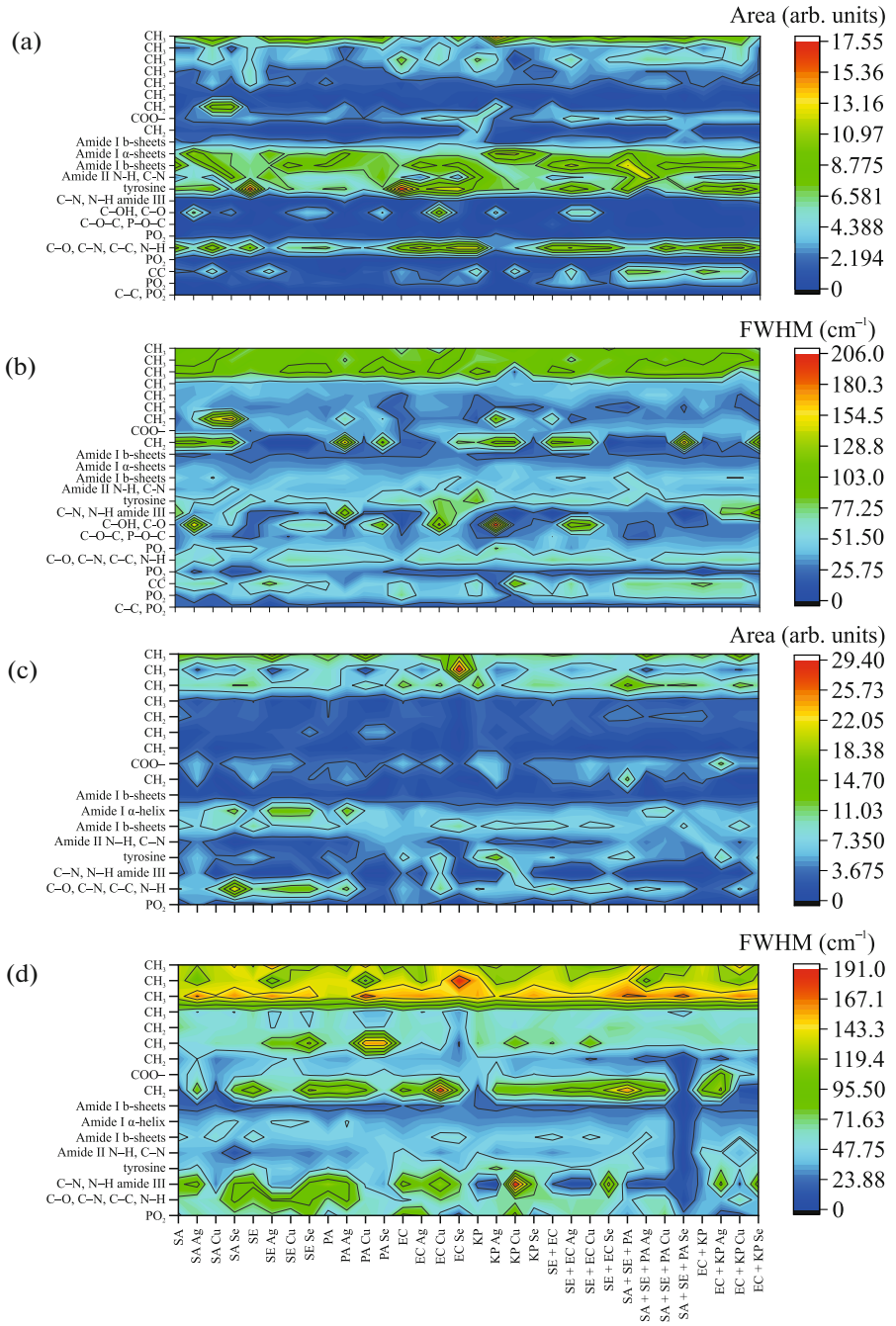

Fig. 4. (Color online) 2D contour maps of the (a, c) area distribution and (b, d) FWHM of IR peaks in (a, b) absorbance and (c, d) optical density spectra corresponding to different molecular vibrations (vertical axis) for bacterial biofilms before and after treatment with silver, copper and selenium NPs (horizontal axis). Control (untreated) biofilms are designated by the abbreviations of the corresponding bacteria: (SA) *S. aureus*, (SE) *S. epidermidis*, (PA) *P. aeruginosa*, (EC) *E. coli*, (KP) *K. pneumoniae*, (SE + EC) *S. epidermidis* + *E. coli*, (SA + SE + PA) *S. aureus* + *S. epidermidis* + *P. aeruginosa*, and (EC + KP) *E. coli* + *K. pneumoniae*. Biofilms treated with silver, copper, and selenium NPs are designated by the abbreviation of the corresponding bacteria with the addition of Ag, Cu, and Se, respectively.

Ag, SA + SE + PA Ag, EC + KP Ag), after treatment with copper NPs (SA Cu, SE Cu, PA Cu, EC Cu, KP Cu, SE + EC Cu, SA + SE + PA Cu, EC + KP Cu) and after treatment with selenium NPs (SA Se, SE Se, PA Se, EC Se, KP Se, SE + EC Se, SA +SE + PA Se, EC + KP Se).

Fourier transform Infrared spectroscopy can detect several possible antimicrobial mechanisms: NPs are

able to change the "fluidity" of the cell membrane by binding to –CH groups in lipids (3100–2800 cm^{-1} region); NPs or ions released from NPs bind to amino acids in proteins, which changes their structure and is reflected in the IR spectra in the range of 1500–1800 cm^{-1}; NPs affect the phosphate groups of nucleic acids in DNA or RNA, which leads to the destruction of their structure, and changes in the spectra are observed in the wavenumber range of 600–1200 cm^{-1}; NP treatment leads to the generation of reactive oxygen species (ROS), which can cause changes in the structures of polysaccharides in the wavenumber range of 900–1200 cm^{-1} [17].

According to the collected data, area of bands, corresponding to the C–C and PO_2 molecular vibrations in DNA and RNA, in the absorbance spectra increased after the NP treatment of SA, SE and PA. In EC and KP biofilms the areas decreased, as well as in all multicomponent biofilms. Bands, corresponding to C–O, C–N, C–C, N–H vibrations in DNA/RNA have initially greater intensities in all samples, and their areas decrease after the treatment with Ag NPs in SA, SE, PA, KP, SE + EC, SA + SE + PA biofilms. Such area decrease may indicate the destruction of the nucleic acids molecular structure [18]. Exopolymers are illustrated by spectral bands of C–OH, C–O vibrations, and their areas increase after NP treatment, with the variation being more prominent for Ag NPs treatment. No changes were detected in multicomponent biofilms SA + SE + PA. Peak ratio A_{1150}/A_{1680} depicts the contribution of carbohydrates C–O in the exopolymer matrix relative to proteins (amide I) [19]. The ratio grows in SA, SE, EC, KP, SE + EC after NPs treatment, which may indicate a more intense production of exopolymers as a defense response to a hostile environment, while the decrease in the peak in PA indicates effective matrix destruction. No significant changes were observed in the remaining combined biofilms.

The main peaks corresponding to molecular vibrations of proteins include tyrosine and amides I and II. The most significant changes are observed for the tyrosine peaks in SE and EC, the area of which decreases after NP treatment, illustrating the disruption of the secondary structure of proteins [20]. The amide II peak has a small area in EC, and this feature is also reflected in combined biofilms with the presence of EC.

The width of the peaks also changes depending on the type of bacteria and their treatment. Thus, the broadening of the C–C peaks in DNA/RNA after treatment with NPs in SE, KP, SE + EC indicates the destruction of the molecular structure. The increase in the width of the peaks corresponding to proteins is clearly evident in EC and EC + KP, which illustrates the possible destruction of their secondary structure in *E. coli*.

Peaks corresponding to membrane lipids largely reflect its integrity [21, 22]. Thus, rigidification (fluidity decrease, hardening) of the membrane was detected in SE, SA + SE +PA.

In the optical density spectra, we observed an increase in the area of DNA/RNA peaks after treatment with copper and selenium NPs in gram-positive bacteria, and a decrease in gram-negative and combined ones, which generally correlates with the data of IR transmission spectroscopy. The peaks corresponding to β-sheets in amide I increase after treatment of gram-negative bacteria and combined biofilms. The contribution of lipids, which correspond to CH_3 vibrations, decreases after treatment with NPs. The width of the peaks corresponding to molecular vibrations in nucleic acids increases after treatment with NPs in SA, SE. The peak corresponding to vibrations in amide III narrows significantly after treatment with silver NPs in SA, SE, EC, SE + EC. In the SA + SE + PA biofilm, the peaks of molecular vibrations in proteins narrow significantly after treatment with selenium NPs. Possible membrane rigidification was observed after treatment with NPs in SA, SE, PA, SA + SE + PA, while in other cases an increase in its fluidity occurred.

It can be seen that the absorption spectra allow more clear differentiation of the peak areas corresponding to amide I and II, while the optical density spectra better demonstrate the distribution of peak widths, and therefore the use of two methods allows obtaining more complete information about the molecular changes occurring in bacterial biofilms.

3.4. Principal Component Analysis of Infrared Spectra

PCA was performed for the IR optical density spectra in the range from 1191 cm to 1800 cm^{-1}, as well as their second derivatives. It was shown that the analysis of second derivatives more accurately differentiates bacteria damaged after NP treatment and viable biofilms (see Figs. 5a, 5b). Positive and negative PC1 values correspond to viable biofilms and to their complete or partial death, respectively (see Figs. 5a, 5b). When comparing PC1 with the IR optical density spectra, the main molecular vibrations responsible for the differentiation of viable cells from nonviable ones are revealed, namely, PO_2, C–O, C–N, C–C, N–H in DNA/RNA; amides I and III; CH_2, CH_3, COO^- in lipids; tyrosine. The decrease in the contribution of α-helices in the spectra of nonviable bacteria is consistent with the Lorentz approximation data of the peaks (see Fig. 5) and may indicate a disruption of the secondary structure of the protein.

Similarly, PCA analysis of the spectra in the range of 2700–3400 cm^{-1} was carried out, which also allowed us to differentiate viable cells from nonviable ones.

Thus, the treatment of bacterial biofilms with silver, copper and selenium NPs can lead to the simulta-

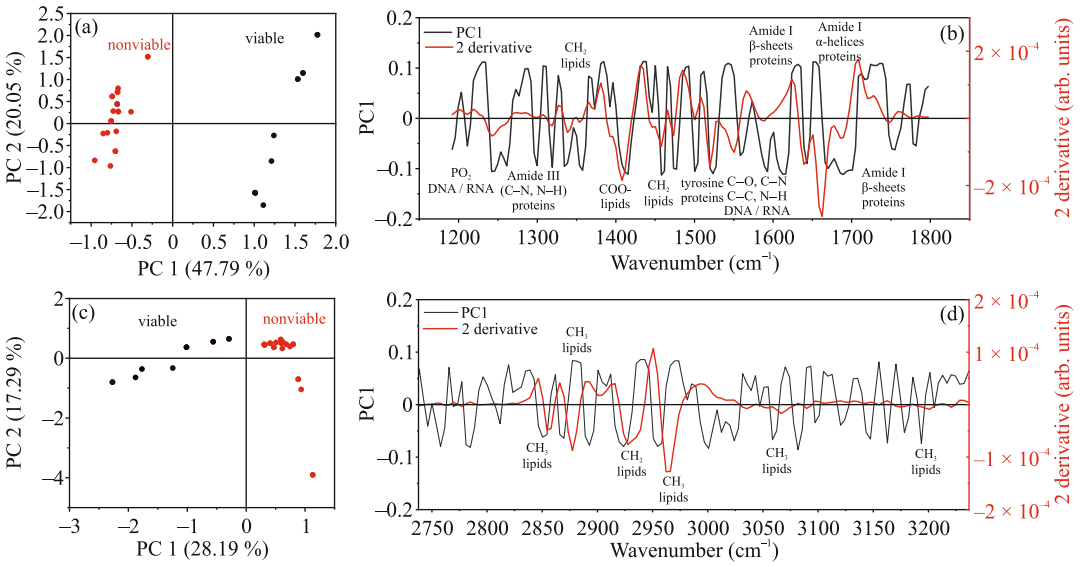

Fig. 5. (Color online) (a, c) Distribution of PC1 components from PC2 and (b, d) comparison of PC1 with second derivative graphs obtained for IR optical density spectra in the ranges of (a, b) 1150–1800 cm^{-1} and (c, d) 2750–3250 cm^{-1}.

neous destruction of the cell membrane, secondary structure of proteins and nucleic acids.

4. CONCLUSIONS

In this work, we have carried out a multiparametric study of the effect of antibacterial nanogels based on nano- and (sub)microparticles of silver, copper and selenium with single- and multi-component biofilms of gram-positive bacteria Staphylococcus aureus, Staphylococcus epidermidis, as well as gram-negative bacteria *Escherichia coli*, *Klebsiella pneumoniae*, and *Pseudomonas aeruginosa*. The nanogels were based on glycerol, silicone oil and Vaseline, which are widespread, biocompatible and inexpensive materials, also suitable for use in wound dressings. The efficiency of glycerol and silicone oil-based nanogels obtained by single-stage LA in viscous media has been demonstrated for the first time using standard biological seeding methods, infrared Fourier transmittance and reflectance spectroscopy, Lorentz peak approximation and PCA analysis. Single-step preparation of gold, silver, copper and selenium NPs in Vaseline was performed for the first time. The reduction in bacterial population has reached from one to four orders of magnitude (99% efficiency). The main cause of bacterial death has been assumed to be damage to the cell membrane, as well as disruption of the structure of proteins and nucleic acids.

SUPPLEMENTARY INFORMATION

The online version contains supplementary material available at https://doi.org/10.1134/S0021364024605190.

FUNDING

This work was supported by the Russian Science Foundation (project no. 24-25-00403, https://rscf.ru/project/24-25-00403/).

CONFLICT OF INTEREST

The authors of this work declare that they have no conflicts of interest.

REFERENCES

1. M. H. Muhammad, A. L. Idris, X. Fan, Y. Guo, Y. Yu, X. Jin, J. Qiu, X. Guan, and T. Huang, Front. Microbiol. **11**, 928 (2020).
2. X. Bai, C. H. Nakatsu, and A. K. Bhunia, Foods **10**, 2117 (2021).

3. L. Shkodenko, I. Kassirov, and E. Koshel, Microorganisms **8**, 1545 (2020).
4. A. S. Joshi, P. Singh, and I. Mijakovic, Int. J. Mol. Sci. **21**, 7658 (2020).
5. S. Ying, Z. Guan, P. C. Ofoegbu, P. Clubb, C. Rico, F. He, and J. Hong, Environ. Technol. Innov. **26**, 102336 (2022).
6. E. Fazio, B. Gokce, A. De Giacomo, M. Meneghetti, et al., Nanomaterials **10**, 2317 (2020).
7. K. A. Altammar, Front. Microbiol. **14**, 1155622 (2023).
8. M. Namakka, M. R. Rahman, K. A. M. B. Said, M. A. Mannan, and A. M. Patwary, Environ. Nanotechnol. Monit. Manage. **20**, 100900 (2023).
9. N. A. Inogamov, V. V. Zhakhovskii, and V. A. Khokhlov, JETP Lett. **115**, 16 (2022).
10. T. V. Malinskii, S. I. Mikolutskii, V. E. Rogalin, Yu. V. Khomich, V. A. Yamshchikov, I. A. Kaplunov, and A. I. Ivanova, Tech. Phys. Lett. **46**, 831 (2020).
11. A. V. Skobelkina, F. V. Kashaev, A. V. Kolchin, D. V. Shuleiko, T. P. Kaminskaya, D. E. Presnov, and P. K. Kashkarov, Tech. Phys. Lett. **46**, 687 (2020).
12. A. Nyabadza, M. Vazquez, and D. Brabazon, Crystals **13**, 253 (2023).
13. A. V. Kabashin and M. Meunier, J. Appl. Phys. **94**, 7941 (2003).
14. S. V. Zabotnov, A. V. Kolchin, F. V. Kashaev, A. V. Skobelkina, V. Yu. Nesterov, D. E. Presnov, L. A. Golovan, and P. K. Kashkarov, Tech. Phys. Lett. **45**, 1085 (2019).
15. P. A. Perminov, I. O. Dzhun, A. A. Ezhov, S. V. Zabotnov, L. A. Golovan', V. I. Panov, and P. K. Kashkarov, Bull. Russ. Acad. Sci.: Phys. **74**, 93 (2010).
16. M. Kansiz, H. Billman-Jacobe, and D. McNaughton, Appl. Environ. Microbiol. **66**, 3415 (2000).
17. F. Faghihzadeh, N. M. Anaya, L. A. Schifman, and V. Oyanedel-Craver, Nanotechnol. Environ. Eng. **1**, 1 (2016).
18. S. Eckhardt, P. S. Brunetto, J. Gagnon, M. Priebe, B. Giese, and K. M. Fromm, Chem. Rev. **113**, 4708 (2013).
19. P. D. Nichols, J. M. Henson, J. B. Guckert, D. E. Nivens, and D. C. White, J. Microbiol. Methods **4**, 79 (1985).
20. W. Jiang, K. Yang, R. W. Vachet, and B. Xing, Langmuir **26**, 18071 (2010).
21. K. Maquelin, C. Kirschner, L. P. Choo-Smith, N. van den Braak, H. P. Endtz, D. Naumann, and G. J. Puppels, J. Microbiol. Methods **51**, 255 (2002).
22. A. A. Kamnev, L. P. Antonyuk, A. V. Tugarova, P. A. Tarantilis, M. G. Polissiou, and P. H. E. Gardiner, J. Mol. Struct. **610**, 127 (2002).

Translated by the authors